Langmuir

Article

pubs.acs.org/Langmuir

Surface-Functionalized Nanoparticle Permeation Triggers Lipid Displacement and Water and Ion Leakage

Priyanka A. Oroskar,[†] Cynthia J. Jameson,[†,‡] and Sohail Murad*[,†,§]

[†]Department of Chemical Engineering, University of Illinois at Chicago, 810 South Clinton Street, Chicago, Illinois 60607, United States

[‡]Department of Chemistry, University of Illinois at Chicago, 845 West Taylor Street, Chicago, Illinois 60607, United States

[§]Department of Chemical and Biological Engineering, Illinois Institute of Technology, 3300 South Federal Street, Chicago, Illinois 60616, United States

ABSTRACT: Functionalized nanoparticles (NPs) are considered suitable carriers for targeted drug delivery systems. However, the ion and water leakage induced by permeation of these nanoparticles is a challenge in these drug delivery methods because of cytotoxic effects of some ions. In this study, we have carried out a series of coarse-grained molecular dynamics simulations to investigate the effect of length of ligands on permeation of a nanoparticle across a protein-free phospholipid bilayer membrane. Water and ion penetration as well as incidence of lipid flip-flop events and loss of lipid molecules from the membrane are explored in this study while varying the nanoparticle size, length of ligand, ion concentration gradient, pressure differential across the membrane, and nanoparticle permeation velocity. Some results from our studies include (1) the number of water molecules in the interior of the membrane during ligand-coated nanoparticle permeation increases with nanoparticle size, ligand length, pressure differential, and permeation velocity but is not sensitive to the ion concentration gradient; (2) some lipid molecules leave the membrane by being entangled with ligands of the NP instead of completing the flip-flop that permits them to rejoin the membrane, thereby leading to fewer flip-flop events; and (3) the formation of water columns or water "fingers" provides a mechanism of ion transport across lipid bilayer membranes, but such ion penetration events are less likely for sodium ions than chloride ions and less likely for nanoparticles with longer-ligands.

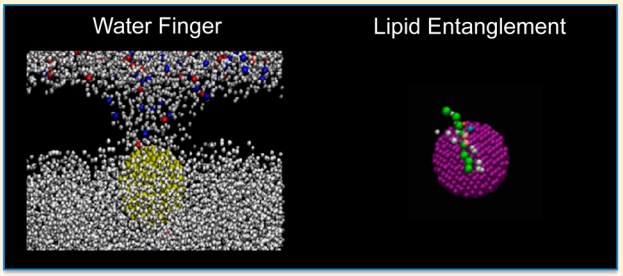

1.0. INTRODUCTION

Biological membranes are a key structural element in the cell and constitute the interface that drug molecules or nanoparticles interact with when passing through the body. How nanoparticles interact with biological membranes is important in determining their applications in biotechnology, drug delivery and phototherapy, among others. Nanoparticles (NPs) designed for these purposes can vary in size and in shape as well as in functionalization.[1−3] Different functional groups can change the surface charge density and hydrophobicity of the nanoparticle.[4,5] Surface modifications with ligands such as butanethiol or octanethiol on gold nanoparticles are an important focus in research.[6] Increasing interest in examining the interaction of nanoparticles and cellular membranes has prompted many studies involving permeation of functionalized gold nanoparticles across lipid bilayer membranes.[7−11] For this present study, we have chosen to examine the permeation of a model lipid bilayer membrane (Figure 1) by a ligand-coated gold nanoparticle (LCNP) to effectively reproduce in simulation an experiment in which a nanoparticle will travel from the extracellular space (Figure 1 compartment A) to the intracellular space (Figure 1 compartment B) under constant velocity. This is significant to many drug delivery applications because the results can be used to predict the effects that nanoparticles can have on the lipid membrane and also the inadvertent transport of extracellular molecules or ions, which may accompany nanoparticle permeation events during their interactions with biological systems.

Previously, we have shown that permeation of a lipid bilayer membrane by a bare gold nanoparticle results in water penetration, ion penetration, and lipid flip-flop events.[12] These effects of nanoparticle permeation can be detrimental to cellular environments and can ultimately result in cell death. We have studied these permeation events under various conditions, such as nanoparticle size, pressure gradient, ion concentration gradient, and permeation velocity of the nanoparticle. Some observations from our previous studies include (1) water leakage into the membrane interior increases with nanoparticle size and pressure differential across the membrane, but is not sensitive to nanoparticle permeation velocity or ion concentration gradient; (2) ion translocation through the membrane is sensitive to the nanoparticle size and ion concentration gradient between the top and bottom

Received: October 7, 2014
Revised: December 8, 2014
Published: December 30, 2014

DOI: 10.1021/la503934c
Langmuir 2015, 31, 1074−1085

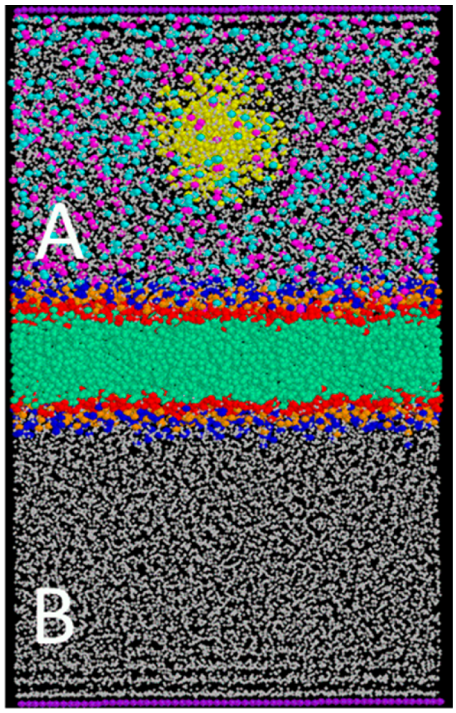

Figure 1. Lipid bilayer membrane simulation system used for examining nanoparticle permeation from the top compartment (A) to the bottom compartment (B) across the lipid bilayer membrane (blue = choline, orange = phosphate, red = glycerol, green = lipid tails, white = water, light blue = chloride, magenta = sodium, gold = nanoparticle core with ligands, purple = impermeable walls).

compartments of the membrane; anion/cation selectivity does not occur for nanoparticle permeation with smaller size nanoparticles, but anion translocation is favored for larger size nanoparticles; and (3) lipid molecule flip-flop events were observed to increase with nanoparticle size and concentration gradient and decrease with nanoparticle permeation velocity and system pressure differential.

In this work, we examine the permeation of a LCNP and its effect on water penetration, ion penetration, and incidence of lipid flip-flop events compared with a bare NP. We vary the pressure gradient, ion concentration gradient, permeation velocity, ligand length, and nanoparticle size to achieve this. It is also worthwhile to note that LCNPs are a realistic representation of nanoparticles in biological systems because the physical characteristics, such as size and shape of nanoparticles synthesized in vitro, is controlled by functional groups present in the environment.[13] Also for in vivo applications, nanoparticles are always found in functionalized form; bare NPs tend to agglomerate and are unlikely to exist as single NPs.[5,13] The results of this work will be of interest to experimentalists who engineer nanoparticles with surface modifications for biomedical applications.

2.0. METHODS

2.1. Coarse-Grained Model. Recently, computer simulations have been used to examine nanoparticle interactions with lipid bilayers.[14−18] In this study, we have used a coarse-grained model of a DPPC lipid bilayer membrane. Coarse-grained models in which small groups of atoms have been treated as interaction sites have been used recently to study many biomolecular systems and are more efficient at extending time scales when compared with atomistic simulations. We use the MARTINI force field developed by Marrink and other collaborators for lipids, surfactants, amino acid and protein applications. It has been proven to accurately reproduce semiquantitatively the fundamental structural and thermodynamic properties of lipid bilayers and proteins.[19,20] Our present system (Figure 1) includes nonbonded, bonded, and charged interactions sites that are all represented by various interaction potentials specific to the type of interaction site (polar (P type), nonpolar (N type), apolar (C type), and charged (Q type)). In the MARTINI force field, nonbonded interactions are modeled using a shifted Lennard-Jones (LJ) potential energy function in which r_{ij} represents the distance between the interacting particle pairs and ε_{ij} represents the depth of the potential well or the strength of a particular interaction.

$$U_{LJ}(r_{ij}) = 4\epsilon_{ij}[(\sigma_{ij}/r_{ij})^{12} - (\sigma_{ij}/r_{ij})^{6}] \quad (1)$$

Most interacting pairs have an effective distance of σ_{ij} = 0.47 nm; for interactions between charged or apolar type molecules, we have used the recommended effective distance of σ_{ij} = 0.62 nm.[20] In our previous studies in which ion concentration gradients are modeled and interactions between charged particles and apolar type molecules were present, the effective distance parameter of σ_{ij} = 0.62 nm was used, as well, and for consistency/comparison, it was important to use the same parameters again. The potential well depth term, ε_{ij}, is specific to the interacting particle types and varies from ε_{ij} = 2.0 to 3.1 kJ/mol for interactions between polar and nonpolar phases (to represent varying degrees of hydrophobic repulsion) and between charged particles with apolar environments. For interactions that are strongly polar, volatile, or nonpolar, such as in aliphatic chains, ε_{ij} ranges from 3.5 to 5.6 kJ/mol. Charged particle type interactions are modeled using the shifted Coulombic potential energy function, where

$$U_{el}(r) = \frac{q_i q_j}{4\pi\epsilon_0\epsilon_r r} \quad (2)$$

Bonded interacting pairs are modeled in the MARTINI force field by a weak harmonic potential function where

$$V_{bond}(R) = \frac{1}{2}K_{bond}(R - R_{bond})^2 \quad (3)$$

and the equilibrium distance, R_{bond}, is 0.47 nm; K_{bond}, the force constant, is 1250 kJ/mol[1] nm[2]. The LJ interaction potential function is not accounted for in bonded interacting pairs. For bonded interacting pairs that have more complex chemical structures, bond angles must be accounted for to more accurately represent the bond configuration. For this, a weak harmonic potential of the cosine type, $V_{angle}(\theta)$ is used for the MARTINI force field model, where

$$V_{angle}(\theta) = \frac{1}{2}K_{angle}[\cos(\theta) - \cos(\theta_0)]^2 \quad (4)$$

2.2. Simulation Setup. The simulation system, (Figure 1) 12.8 × 12.6 × 22.2.0 nm in size, consists of 512 dipalmitoylphosphatidylcholine (DPPC) molecules and ∼23 000 CG water molecules. We have previously observed that this lipid membrane system self-assembles from an isotropic solution of lipids in a coarse-grained simulation.[21] In that study, the properties of this self-assembled bilayer are found in good agreement with experimental measurements, which validates the effectiveness of the simulation model we are using. Our simulation system contains two walls impermeable to water and ions that are cut from a face-centered cubic (FCC) structure. The two impermeable walls, which separate the aqueous compartments A and B (see Figure 1), were inserted in the top and bottom of our model system to maintain pressure differentials across the membrane. The LCNP structure was obtained through a cycled annealing procedure in which butanethiol ligands are attached onto the nanoparticle, as we have shown previously.[22] However, the cytotoxicity of these nanoparticles has been shown to be size-dependent and different chemical properties of functional groups on the nanoparticle can have negative effects inside various biological environments.[23,24] For our simulations, we use smaller nanoparticles between 1.0 and 3.0 nm in diameter; however, in the current study, we focused on functionalized nanoparticles 2.0 and 3.0 nm in diameter. The nanoparticles

DOI: 10.1021/la503934c
Langmuir 2015, 31, 1074−1085

functionalized with butanethiol ligands $[CH_3(CH_2)_{n-1}SH]$ are designated as short-length LCNP, or SL-LCNP, when ligands have n = 4 and long-length LCNP, or LL-LCNP, when n = 8. The 2.0 and 3.0 nm in diameter LCNP with 87 butanethiol ligands annealed to each nanoparticle have a surface coverage of 48.3% and 41.0%, respectively. Experimentally, the surface coverage of a 2.0 nm diameter alkanethiol-coated nanoparticle achieved is between 52 and 57%, and for a 3.0 nm diameter ligand-coated nanoparticle the experimental surface coverage is ∼50%.[25] For larger diameter nanoparticles up to 5.0 nm diameter, the experimental surface coverage achieved can approach as low as 24% because of steric hindrance of alkanethiol ligands on the nanoparticle surface.[25]

The parameters varied in this work include ligand length, nanoparticle size, ion concentration gradient, pressure gradient, and nanoparticle velocity. For simulations with unequal ion concentrations, ions were added to compartment A of the system at a concentration of 1.4 mol % (the saturation limit of sodium chloride in water is 1.8 mol %). Systems with pressure differentials up to 300 bar were studied in this work (corresponding to systems at press0 (0 bar)/press1 (100 bar)/press2 (200 bar)/press3 (300 bar)). We have previously shown that the equilibrium thickness of our lipid membrane at 0 bar is 3.78 nm, which is close to the experimental thickness (3.85 nm) of a DPPC lipid bilayer membrane (the thickness is measured as the distance between equilibrated phosphate groups on the top and bottom leaflet of the lipid bilayer membrane).[12] To construct membranes under varying pressure differentials, the top wall is moved toward the lipid bilayer membrane at a constant velocity of 0.025 m/s for 10 ns, and then the system is allowed to equilibrate for another 10 ns. Pressure differentials were estimated from the force required to hold the tethered membranes. Three systems with varying pressure differentials were investigated by repeating this procedure three times in which the wall is moved for 10 ns, stopped, and the membrane is allowed to equilibrate for 10 ns. In actual experiments examining lipid membrane permeation, phospholipid membranes are supported on solid surfaces such as polymers[26] to imitate the role of the extracellular matrix in vivo. We have replicated this solid support by tethering boundary lipid molecules to their initial position in the DPPC phospholipid bilayer using a harmonic spring force. These tethered molecules extend 1 nm from the end of the simulation box and comprise 8% of the total membrane width. Tethering lipid molecules in the DPPC phospholipid bilayer allows the pressure differential to be maintained. The thickness of the membrane under a 300 bar pressure differential shrinks by only 3.2%, which shows that the structure of the membrane does not change significantly for the systems under the pressure differentials used in this work. We recognize that the pressure differentials modeled in our study are significantly larger than those observed biologically; however, to investigate the pressure effects within the time constraints of a simulation, we studied these higher pressure. The goal was to identify only any role pressure could play in the processes investigated here. Clearly, if these high pressures do not result in any change (which was observed in many cases), then it is unlikely that lower pressures actually encountered in living systems will play any role.

Several nanoparticle velocities were studied (0.35, 0.525, 0.7, and 1.0 m/s designated as velocities V1, V2, V3, and V4, respectively). Although the nanoparticle velocities studied in this work are larger than typical nanoparticle velocities in some experimental studies, they are still a few orders of magnitude lower than the thermal velocities of nanoparticles at the simulation system temperature. The root-mean-square velocity of experimental alkanethiol-protected nanoparticles of range 1.0-3.0 nm in diameter at the examined system temperature of 323 K is 6.64-24.63 m/s. The root-mean-square velocity of sodium and chloride ions, water, and lipid molecules at the system temperature ranges from 52.32 to 334.37 m/s. Thus, the chosen velocities for the present LCNP study are realistic representations of the nanoparticle permeation process while advantageous for practical simulation times. We have also demonstrated previously that the DPPC membrane recovers after two nanoparticle permeation cycles at the chosen velocities,[27] which suggests that the membrane is not compromised at the studied velocities. In our simulations, the gold nanoparticle (moving at fixed velocity) with annealed surface sulfur atoms is pulled by its center of mass with ligands allowed to move freely. In experimental settings where nanoparticles studied are often 10−100 nm in diameter, even larger minimum driving forces may be needed compared with nanoparticles examined in the present study. Velocities similar to the ones used in our study have been investigated recently in many applications involving nanoparticles in drug delivery systems. Magnetic nanoparticles (MNPs) as nanocarriers delivered through a magnetized stent have been explored computationally and experimentally to determine the effect of NP size and velocity on capture efficiencies of these MNPs.[28,29] For delivery through a magnetized stent, the MNP size and velocities examined in these studies ranged from 25 to 350 nm in diameter and 0.05 to 0.7 m/s, respectively.[28,29] For comparison, the typical flow in an artery ranges from 0.15 to 0.2 m/s, and nanocarriers 10−100 nm in diameter are readily transported in vivo during blood circulation.[30−32] In addition, others have examined the collision interaction of Janus nanoparticles (nanocarriers for drug delivery systems) and lipid vesicles in simulation when the initial velocity of the nanoparticle varied between 0.257 and 1.626 m/s.[33]

Nanoparticles while permeating the lipid bilayer induce pores inside the membrane, which result in the transport of both water and ions during the lifetime of the pore, which generally spans about 50−100 ns. The diameter of the pore is strongly dependent on the nanoparticle size and, to some extent, on the velocity of the permeating nanoparticle. In experimental settings, pores are induced in lipid membranes with various analytical methods, such as application of mechanical stress from pipet aspiration or application of an electric field (electroporation).[34,35] Changing the magnitude of mechanical or chemical stress applied to the lipid membrane can vary the size of these pores. In some cases, large hydrophilic pores may form that continue to grow and become stabilized in the bilayer membrane,[35] which hinders membrane recovery. The simulations were carried out using the LAMMPS simulation package,[36] and the MARTINI coarse-grained model[20] was used for the force field parameters and nonbonded pair coefficients. Parameters involving the butanethiol-protected gold nanoparticles are given in our previous work.[22] The simulation time step was 10 fs to ensure stability of the membrane system. A Langevin thermostat was used to maintain temperature at 323 K with the NVE ensemble time integrator, and periodic boundary conditions were applied to our system.

3.0. RESULTS AND DISCUSSION

The formation of nanoscale pores in lipid membranes arising from nanoparticle permeation have been observed experimentally as well as in simulation[4,37−40] and also in our previous simulations of nanoparticle (both bare and ligand-coated) permeation across lipid bilayer membranes.[12,22,27] Water and ion leakage as well as lipid flip-flop have been observed to occur in simulation across a water pore or defect in a lipid membrane.[41−46] The following results in the present study illustrate the impact of LCNP permeation on DPPC lipid bilayer membranes: water and ion penetration, lipid flip-flop, and lipid loss. We compare and contrast this to the effect of bare NP permeation.

3.1. Water Penetration. In the present study, we have examined water penetration more closely and investigated the dependence of water penetration on ligand length, nanoparticle size, permeation velocity, pressure differential across the membrane, and ion concentration gradient. Water penetration occurs during nanoparticle permeation in which water molecule movement is facilitated by pore formation and defects induced by the nanoparticle. Water penetration as examined in this study is defined in terms of the number of water molecules originally in either compartment of the system that are later found in the hydrophobic interior of the membrane during nanoparticle permeation across the lipid bilayer membrane.

DOI: 10.1021/la503934c
Langmuir 2015, 31, 1074−1085

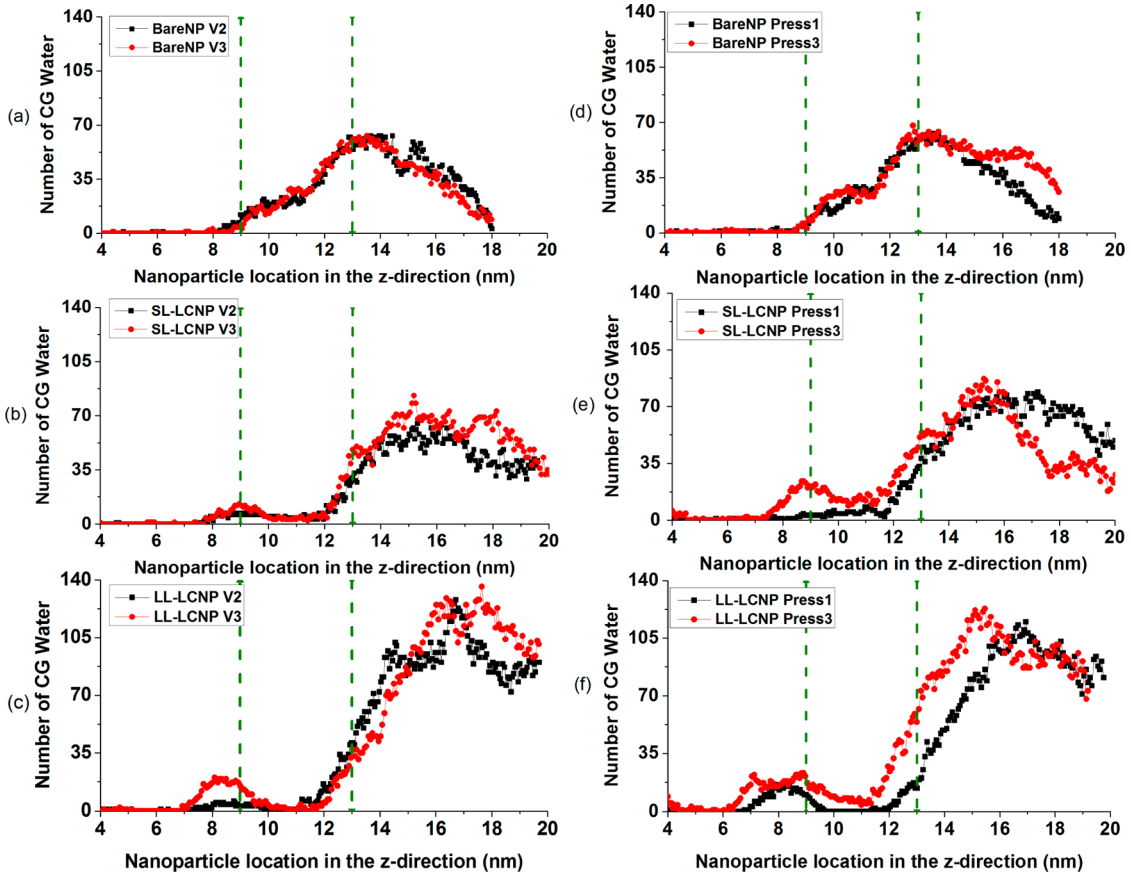

Figure 2. Number of CG water molecules found in the hydrophobic membrane interior with 2.0 nm diameter NPs under the following conditions: (a–c) Effect of nanoparticle velocity and ligand length: press1, no concentration gradient. (d–f) Effect of pressure differential and ligand length: no concentration gradient, V3 (0.7 m/s). The green dotted lines represent the equilibrated position of the phosphate groups in the DPPC lipid bilayer membrane.

The hydrophobic interior is defined here as the region extending 0.75 nm from the center of the lipid bilayer membrane; for the membrane at equilibrium, this includes the lipid tail region. The water molecules located at the openings of the water pore are not counted.

Before discussing the effect of conditions being varied, we note some characteristic differences between the bare NP and LCNP. When the LCNP is permeating the membrane, water molecules start to move into the hydrophobic interior of the membrane when the ligands of the nanoparticle are located at the position of the phosphate groups on the lipid bilayer membrane. At this point, the core of the nanoparticle is still outside the bilayer membrane. This is in contrast to the case of the bare NP permeation, where water penetration occurs only when the bare NP is at the position of the phosphate groups in the bilayer membrane. This early onset of water migration into the pore occurs because mobile ligands attached to the leading edge of the LCNP disturb the membrane ahead of the gold core by pushing lipids apart, thereby making room for the nanoparticle inside the membrane. The number of water molecules found inside the hydrophobic membrane interior increases as the LCNP moves farther into the membrane. The number of water molecules moving from compartment A to the hydrophobic membrane interior decreases slightly as the LCNP approaches the tail region of the first membrane bilayer but then increases significantly as it approaches the tail region of the second membrane bilayer. We believe this initial decrease is in part due to the LCNP occupying enough space inside the water pore so that there is little room for water molecules to leak into the membrane interior.

After the LCNP passes the first leaflet and the nanoparticle core is inside the membrane interior, a pore is still is visible from the top view of the first leaflet. Because of the favorable interaction of the ligands and the hydrophobic phospholipid tails, however, there is no space available inside the membrane interior for water molecules at this stage. The number of water molecules moving to the hydrophobic interior from either compartment does not reach a maximum until the ligands of the LCNP have completely left the membrane. This is in contrast to the permeation of the bare NP, for which the maximum number of water molecules penetrating from both compartments occurs when the nanoparticle has just moved past the position of the phosphate groups of the second layer of the membrane. The late occurrence of the maximum in the water number density in the membrane interior occurs for the LCNP because ligands are still entangled inside the head groups of the membrane's second layer, even though the nanoparticle core has exited the second layer; thus, water permeation continues to occur as a result of the delayed disturbance of the membrane.

After the LCNP exits the second layer of the membrane, the water molecules that permeated into the hydrophobic interior start to move out of the membrane. The expulsion of the water molecules occurs because the hydrophobic environment is not attractive to water molecules and also because the lipid molecules tend toward equilibrium, their original configuration

DOI: 10.1021/la503934c
Langmuir 2015, 31, 1074–1085

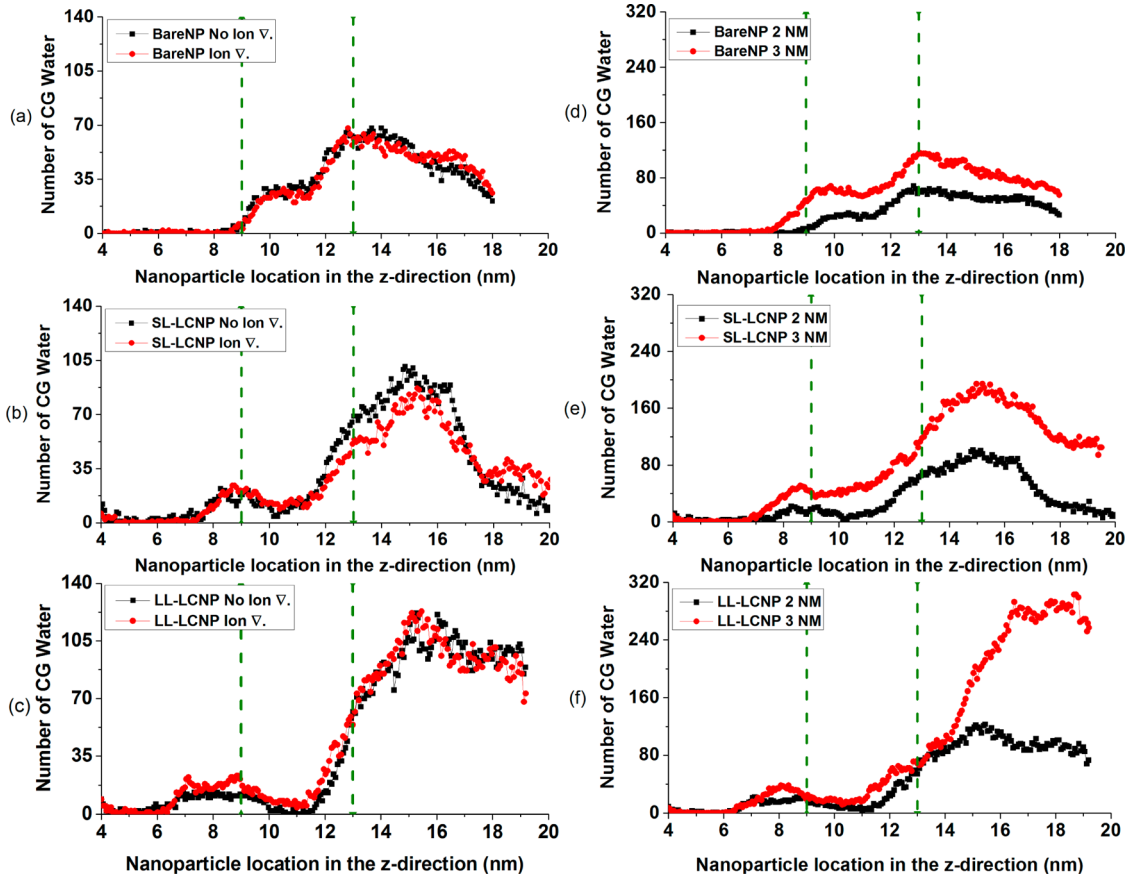

Figure 3. Number of CG water molecules found in the hydrophobic membrane interior under the following conditions: press3, V3(0.7 m/s). (a−c) Effect of ion concentration gradient and ligand length, obtained from 2.0 nm diameter nanoparticles. (d−f) Effect of nanoparticle size and ligand length with ion concentration gradient. The green dotted lines represent the equilibrated position of the phosphate groups in the DPPC lipid bilayer membrane.

where the hydrophilic head groups and hydrophobic tails are packed together; this starts the recovery of the lipid bilayer membrane. The ligands attached to the gold core become entangled in the headgroup of the second layer of the membrane, thereby disturbing the membrane significantly more in comparison with permeation with a bare gold particle. For each of the results in Figures 2 and 3, each simulation was observed for 30 ns under the designated conditions.

At 30 ns, the number of water molecules found in the hydrophobic membrane interior in the present study is significantly larger than in the case of the bare NP, which indicates that the membrane has not yet fully recovered after permeation by a LCNP, whereas for the bare NP permeation studies, the membrane does recover within 30 ns under most conditions. Complete membrane recovery (zero water molecules found in the hydrophobic interior) can be established by allowing the system to equilibrate after the nanoparticle permeation cycle is complete. Our simulations did not run long enough to achieve complete recovery, but there are clear indications that the recovery process has begun.

Characteristics of the LCNP (size and ligand length) affect the water permeation. As observed in Figure 3d−f, with a 3.0 nm diameter nanoparticle, more water molecules are found in the membrane interior than compared with permeation with a 1 or 2.0 nm diameter nanoparticle. With a larger nanoparticle size, the internal structure of the membrane is disturbed more (results not shown), as indicated by the local order parameter. We have previously shown that the local order parameter is elevated for larger nanoparticles disturbing the membrane structure.[12] During permeation of a 3.0 nm diameter nanoparticle, these effects are even more pronounced when the nanoparticle is functionalized with ligands and stay consistent for larger nanoparticles with increased ligand length. Within the 30 ns simulation, the membrane recovery process is initiated later with a larger nanoparticle because the integrity of the membrane is disturbed more.

We now report our observations for the effect of permeation velocity, pressure differentials, and ion concentration gradients. As seen in Figures 2 and 3, the number of water molecules originally from either compartment that are found in the hydrophobic interior of the membrane increases with increasing ligand length. Longer ligands cause more disturbances to the membrane structure and increase the number of water molecules permeating from either compartment into the hydrophobic interior of the membrane. The longer ligands cause more disturbances also to the head groups of the second layer of the membrane; therefore, in the 30 ns simulation time, the lipid membrane has recovered the least after permeation by a LL-LCNP as compared with permeation by the short length LCNP.

The number of water molecules moving into the membrane interior from either compartment increase with LCNP permeation velocity when the nanoparticle has passed the second leaflet of the membrane (no effect was found in the previous study with bare NPs). Initially, the number of water molecules in the membrane interior is relatively constant at

DOI: 10.1021/la503934c
Langmuir 2015, 31, 1074−1085

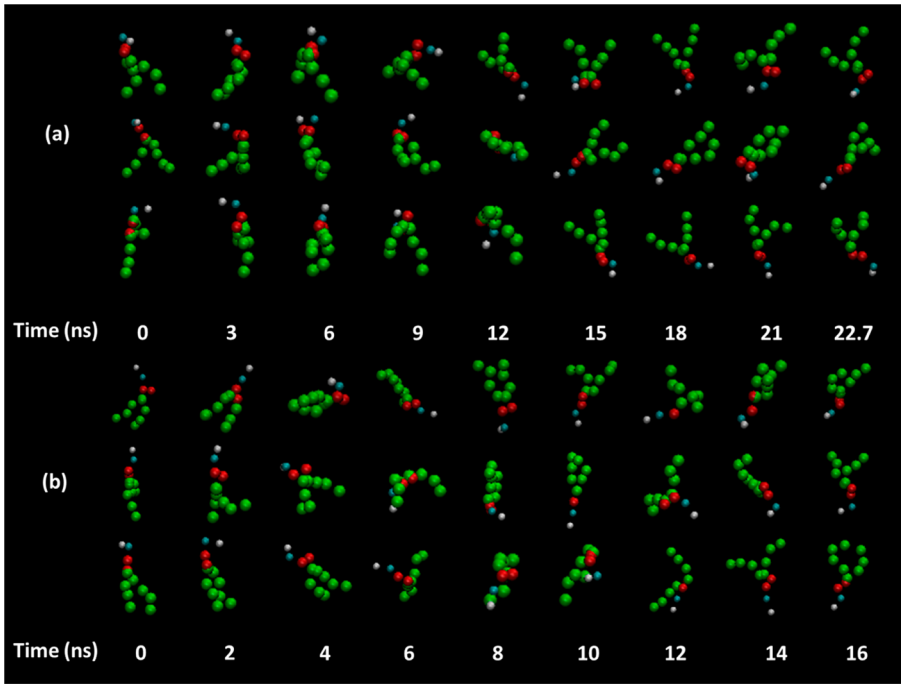

Figure 4. Typical lipid flip-flop event trajectories for a SL-LCNP that are obtained from 3.0 nm diameter NPs, for a press1 system under ion concentration gradient, and nanoparticle velocities of (a) 0.7 and (b) 1.0 m/s.

varying velocities; however, at higher nanoparticle velocities, ligands cause more disruption to the membrane, which results in the formation of a larger water pore. As indicated by Figure 2a–c, this facilitates an increase in water molecules moving into the hydrophobic interior of the membrane. Indeed, it was found that at higher velocities, the membrane recovery is lower (in the 30 ns simulation time) than at lower velocities. This effect is largest for the longer length ligands.

The number of water molecules moving into the membrane interior increases when the nanoparticle is permeating systems under higher pressure differentials. The minimum force on the NP required to maintain a constant velocity for the nanoparticle is larger for systems under higher pressures. Thus, the nanoparticle causes more damage to the first layer of the membrane bilayer, which in turn results in an increased amount of water leakage into the membrane interior. This is consistent for both LCNPs and bare NPs. For LCNPs, the water leakage into the membrane interior is larger than in the case of the bare NP because of the ligands' disturbing the integrity of the membrane more at larger system pressures, as seen in Figure 2d–f. However, for systems under higher pressure differentials, the lipid membrane recovery process is initiated sooner within the 30 ns simulation time than compared with systems under lower pressure differentials (also found during permeation of bare NPs). For systems under greater pressure differentials, the water molecules from compartment A that entered the membrane interior during nanoparticle permeation are at a higher pressure than water molecules in compartment B. Consequently, the water inside the membrane interior has greater propensity to be pushed out of the lipid membrane interior, and the recovery process of the membrane is initiated sooner compared with no applied pressure. This effect is greatest for long-length ligands.

Ion concentration gradients across the membrane do not affect the amount of water leakage (this was also found in our earlier studies using bare NPs). As observed in Figure 3a–c, water leakage into the membrane interior is not sensitive to the ion concentration gradient because the chemical potential driving force across the lipid bilayer membrane is very weak (compartment A is a 1.4 mol % saturated NaCl solution).

3.2. Lipid Flip-Flop Events. In a lipid flip-flop event, a lipid molecule translocates from one leaflet of the membrane to the other across the lipid bilayer. This does not often occur spontaneously and is aided by lipid translocators such as enzymes or integral membrane proteins.[47] Studies indicate that intrinsic membrane proteins may hasten the lipid flip-flop process due to formation of defects or sinks in the lipid bilayer.[48] Lipid flip-flop is a biological process integral to cells which has consequences on the naturally asymmetric or heterogeneous distribution of lipids on the extracellular or intracellular membrane leaflet.[49]

In the present study, we examined the lipid flip-flop events accompanying the permeation of the lipid bilayer by a ligand-coated nanoparticle under varying conditions. In each counted event, a lipid molecule from the top leaflet of the lipid bilayer membrane moves through the water pore induced by the LCNP and is found in the lower leaflet of the membrane at the end of the permeation cycle. First, we closely examine the molecular details of how a flip-flop event occurs and discover whether this mechanism is affected by characteristics of the nanoparticle itself, that is, size and ligand length. Next, we observe the mechanism in which a lipid molecule is removed from the top leaflet of the membrane but does not complete the process of joining the lower leaflet; instead, it gets dragged away from the membrane entirely (these are not included in the events counted as flip-flops) entangled in the ligands of the NP. We identify those lipid molecules that are removed from the top and bottom leaflets of the bilayer and investigate how the number of these displaced lipids varies with nanoparticle size and ligand length. Last, we summarize the effects on the number of flip-flop events from nanoparticle characteristics and

DOI: 10.1021/la503934c
Langmuir 2015, 31, 1074–1085

system conditions (ion concentration gradient, applied pressure, choice of velocity).

3.2.1. Details of a Lipid Flip-Flop. In Figure 4a,b, we show the snapshots of typical lipid flip-flop events as observed in our simulations for a nanoparticle with short ligands moving through the bilayer at (a) 0.7 and (b) 1.0 m/s.

We chose not to display snapshots of lipid flip-flop for the LL-LCNP studies because too few events were observed. A flip-flop is completed in 15−40 ns, depending on the established nanoparticle velocity (the time scale of lipid flip-flop events is always dependent on the nanoparticle velocity because the water pore formed in the membrane through nanoparticle permeation has a certain pore lifetime, as we have seen in previous work[12]). All lipid flip-flops observed in our simulations occurred by the same mechanism: the lipid molecule undergoes a full rotation or reorientation in the *z*-direction from the top membrane leaflet to the bottom membrane leaflet through the water pore. Figure 5 shows the angle between the DPPC

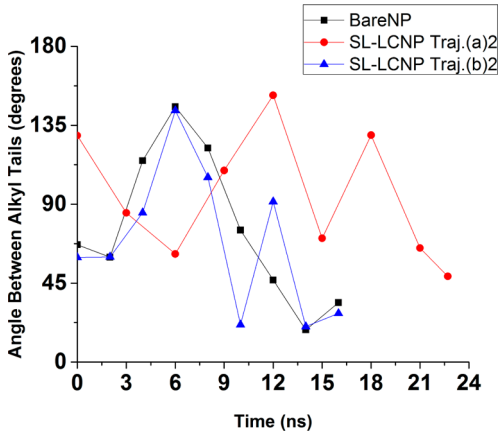

Figure 5. Angle analysis of the alkyl tails of a typical lipid flip-flop (corresponding to the same flip-flop events pictured in Figure 4).

phospholipid tails throughout the course of a complete lipid flip-flop event (pictured in Figure 4; trajectory (a)2 and (b)2 correspond to the second snapshot shown of a typical lipid flip-flop for nanoparticle velocity of 0.7 and 1.0 m/s, respectively) . In this full rotation, the tails of the lipid molecule open as the lipid head begins to turn over, at which point the tails begin to come back together again. For the LCNP, a variation of the flip-flop mechanism from the bare NP is observed: the alkyl tails undergo slight fluctuations of movement where the tails open and close (several times in some cases) before completing the reorientation as the hydrophobic alkyl tails get entangled in the hydrophobic ligand groups. This is in contrast to the bare NP case in which the alkyl tails open, stay open during the rotation, and do not close until the lipid molecule has completely reoriented. . Examples are shown in Figure 5. Furthermore, in the bare NP case, the lipid head of the flip-flopping molecule tends to stay facing the nanoparticle, and alkyl tails tend to face toward the bottom membrane leaflet until the flip-flop is completed. In the ligand-coated case, the alkyl tails of the lipid molecule undergoing the flip-flop event stays entangled with the ligands of the LCNP until it is able to move to the bottom leaflet of the membrane and complete the reorientation.

3.2.2. Loss of Lipids from the Membrane. A few lipid molecules do not undergo the typical lipid flip-flop event but are instead dragged into the bulk solution entangled with the ligands of the nanoparticle. Figure 6 shows the mechanism by which this can occur. As the particle approaches the top leaflet,

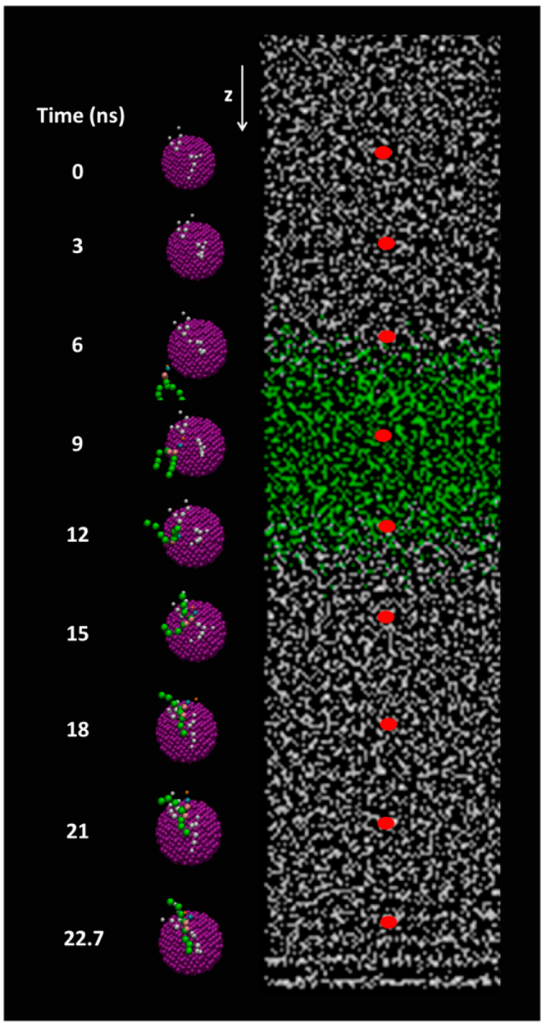

Figure 6. Snapshots of the mechanism by which a lipid molecule is dragged to the bulk solution by entanglement with ligands on the nanoparticle (for clarity, the other ligands on the nanoparticle are not shown). The red dots represent the position of the nanoparticle at each snapshot.

the lipid molecule begins to interact with the ligands on the nanoparticle and continues to adhere to the ligands of the nanoparticle as the latter moves through the membrane and passes the second leaflet. In this figure, we identify four ligands that come within the interaction volume of the lipid (for clarity we do not display the other ligands). All lipids that started but did not complete the flip-flop (such as the one shown in Figure 6) are observed to associate with the same group of ligands on the nanoparticle throughout the permeation. The lipid becomes entangled with a pair of ligands close to one or other of the two lipid tails and is dragged along by the nanoparticle. This effectively mimics the configuration that a DPPC molecule would have in the membrane at equilibrium, where its tail pair is surrounded by a group of other hydrophobic tails. Because of this favorable hydrophobic interaction between the lipid tails and the alkane ligand, the ligands on the nanoparticle assembly essentially compete for favorable hydrophobic interactions with the tails of the second leaflet of the bilayer, which the lipid would join to complete a flip-flop. When the lower leaflet wins

DOI: 10.1021/la503934c
Langmuir 2015, 31, 1074−1085

out, a flip-flop event is completed; otherwise, the entangled lipid continues to move through the pore along with the ligand-coated nanoparticle to the bulk solution and is lost from the membrane. This entanglement becomes more severe with longer ligands and larger nanoparticles, which is consistent with our finding that for LCNPs, fewer number of flip-flops are observed with longer ligands.

Figure 7 shows the incidences of lipid molecules lost from both leaflets of the membrane under various conditions. We

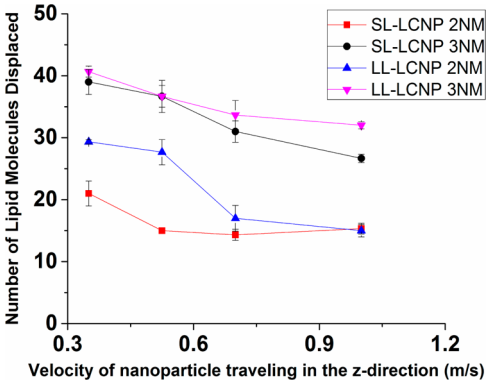

Figure 7. Number of lipid molecules lost from both bilayer membrane leaflets for a system with ion concentration gradient, as a function of velocity (for the press1 case). The error bars are based on three independent simulations.

observe more lipids lost from the membrane for the larger diameter nanoparticle. This shows that larger nanoparticles with increased surface area have a higher propensity to extract lipids from the membrane, which can be attributed to the larger water pore formed during permeation. With increasing ligand length, in most cases, the number of lipid molecules lost from both membrane leaflets increases; the longer alkyl ligands result in a more favorable entanglement of the lipid molecule because of the higher ligand density, thereby increasing the incidences of the lipid being dragged away from the membrane. We also observe that significantly more lipid molecules are lost from the lower membrane leaflet compared with the top leaflet; this is consistent with results on a previous coarse-grained investigation of the penetration of a DPPC lipid bilayer by single-walled carbon nanotubes.[50]

The bare nanoparticle also has been found to drag lipid molecules from both leaflets through the water pore to the bulk solution on the other side of the membrane, where the lipid essentially plays the role of a ligand adhered to the particle, but these incidences are fewer. The lipid head tends to stay facing the bare gold particle while the tails point away, favoring the completion of a flip-flop in comparison with the ligand-coated particle.

With decreasing nanoparticle velocity, we observe in most cases that the number of lipid molecules removed from the bilayer tends to increase. Experimentally, the nanoparticle velocities studied in nanoparticle permeation are often smaller than those examined in this study. Since we observed a clear trend in Figure 7 that lipid molecule removal increases with decreasing velocity, it is likely that lipid extraction will occur in experimental nanoparticle permeation studies. The loss of lipid molecules from a membrane leaflet can be detrimental to the integrity of the membrane and in some cases could be more harmful than lipid flip-flop. If the loss of lipid molecules becomes too great, the membrane may be unable to recover, and this can result in cell death.

3.2.3. Number of Lipid Flip-Flop Events under Various Conditions. For all conditions, the number of flip-flop events for LCNPs is smaller than for a bare NP. With increasing nanoparticle size, more lipid flip-flop events are observed in the case of both bare NP and LCNPs, as shown in Figure 8a,b in systems under an ion concentration gradient. This is expected because at higher nanoparticle sizes, the water pore is larger, and greater water penetration and ion transport occurs because the water pore is stabilized by the discharge of the transmembrane ionic charge balance.[45] This allows for the increased number of lipid flip-flop events to occur, too, especially for the bare NP. The "entanglement" effect discussed above is more pronounced in the LL-LCNP, as compared with the SL-LCNP, and as a result of this, fewer flip-flop events are observed for increasing ligand-lengths. As observed previously in the case of the bare NP, under most conditions, the number of lipid flip-flop events during permeation of a LCNP reaches a limiting value with increasing velocities.[12] At higher velocities, the permeating nanoparticle induces a water pore with a shorter lifetime in the membrane, which decreases the available time for lipid flip-flop events to occur.

3.3. Ion Penetration. Ion permeation across lipid bilayer membranes has been suggested to take place via various mechanisms, including pore-mediated, assisted transport,

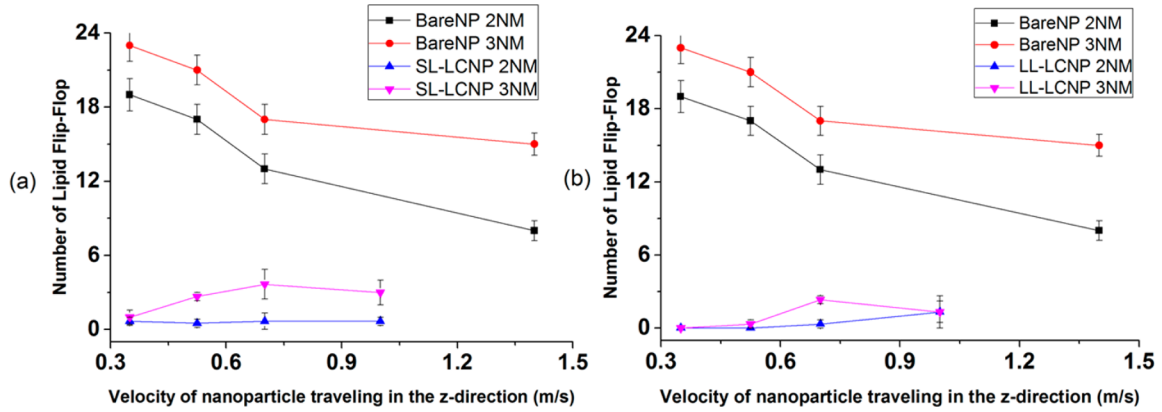

Figure 8. Effect of ligand length and nanoparticle size on the number of lipid molecule flip-flop events examined under an ion concentration gradient, press1, varying nanoparticle velocity. The error bars are based on three independent simulations.

DOI: 10.1021/la503934c
Langmuir 2015, 31, 1074−1085

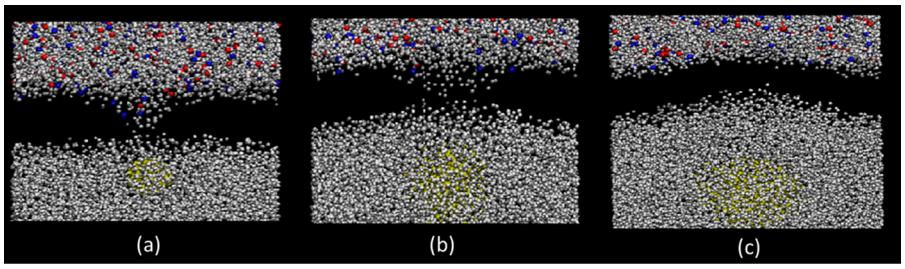

Figure 9. Snapshots of ion concentration gradient simulation system for 2.0 nm diameter (a) bare NP, (b) SL-LCNP, and (c) LL-LCNP at maximum water leakage observed. The water molecules are shown in white; the nanoparticle and ligands, in yellow; and the sodium and chloride ions, in blue and red, respectively.

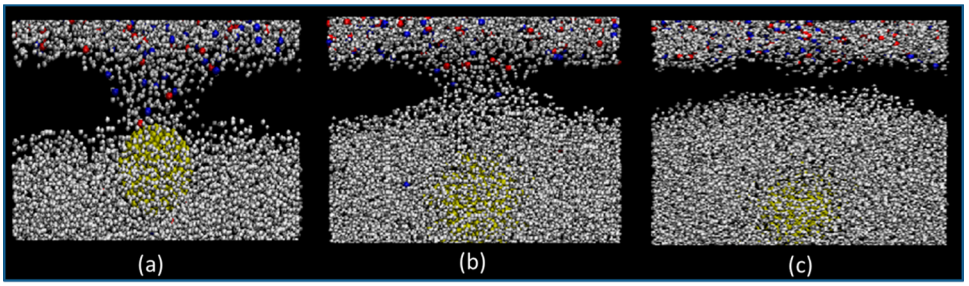

Figure 10. Snapshots of ion concentration gradient simulation system for 3.0 nm diameter (a) bare NP, (b) SL-LCNP, and (c) LL-LCNP at maximum water leakage observed. The water molecules are shown in white; the nanoparticle and ligands, in yellow; and the sodium and chloride ions, in blue and red, respectively.

solubility diffusion, and lipid flip-flop.[51] In the present study, we focused on pore-mediated ion penetration through a water pore created by nanoparticle permeation across a lipid bilayer membrane.

Ions present in the aqueous solution outside the membrane cannot permeate the membrane on their own as a result of the Coulombic interaction between the ions and the charged head groups on the phospholipid. Because the interior of the membrane is highly hydrophobic, the ions are confined to the phospholipid head groups and cannot penetrate the membrane. Ions may permeate across the membrane along with the water molecules as the nanoparticle creates the water pore. In this study, we have examined the effect of nanoparticle size, ligand length, pressure gradient, and permeation velocity on the selectivity and ion penetration rate. During nanoparticle transport through the membrane, a pore is created through which water can transport to the membrane interior, as shown previously. Along with water permeation, some ions may move across the membrane through the water pore. Although a majority of the ions that enter the pore during nanoparticle permeation will eventually return to the bulk solution, a few move along the water pore and completely cross both layers of the lipid bilayer membrane. Similar to what we have seen for water permeation, the maximum number of ions found in the membrane occurs when the nanoparticle is exiting the second layer of the membrane.

In the present study, an ion penetration event is defined as the movement of a sodium or chloride ion from compartment A of across the lipid bilayer membrane to compartment B. We conducted a large number of nanoparticle permeation simulations under a concentration gradient and examined 42 independent simulations where ion penetration events were observed. It appears that nanoparticle size is important for ion penetration events to be observed.

In the case of the smaller (2.0 nm) LCNP, we find that there were almost no ion penetration events observed under varying conditions, and ion permeation was not sensitive to changing pressure gradient, increasing velocity (all true also for the bare NP), or ligand length because there are few water molecules to drag the ions along. Since permeation by a 3.0 nm diameter nanoparticle results in a larger water pore and increased water leakage to the membrane interior sometimes accompanied by lipid flip-flop events, ion penetration events are expected to increase, as well. Indeed, we find in the present study that ion penetration events are observed during permeation of a 3.0 nm diameter LCNP, although fewer than for a 3.0 nm diameter bare NP and fewer yet when ligand length is increased. This can be attributed to the hydrophobicity of the ligands augmenting the hydrophobic environment of the membrane interior: more ions return to the water/membrane interface, where they can bind to the lipid head groups instead of passing through the entire membrane.

Previous theoretical investigations of ion permeation through a water pore in a bilayer have observed the existence of "water fingers" or a chain of linked water molecules that protrudes through the bilayer from one aqueous compartment to the other.[51−55] In agreement with prior atomistic molecular dynamics work,[51,55,56] we observed in our simulations that ions permeating the lipid membrane from compartment A to B travel along the water molecule network to cross the bilayer membrane. Previous work indicates that the chloride ion is able to integrate into a water molecule network by forming hydrogen-bonded bridges with surrounding water molecules.[57] This agrees with our findings that chloride ions are readily accepted into the "water finger" network of water molecules and permeate the lipid bilayer membrane more often than sodium ions. Many studies, including our previous work, have indicated that sodium ions have a tendency to stay in the lipid membrane headgroup region near the choline and phosphate

DOI: 10.1021/la503934c
Langmuir 2015, 31, 1074−1085

groups (because of stronger Coulombic interactions), whereas the chloride ion tends to be at the interfacial region close to the lipid membrane.[12,51] Therefore, sodium is less likely to permeate the membrane along the "water finger" network, and as a result, more chloride ions permeate the lipid membrane compared with sodium ions. We observed this selectivity for chloride ions over sodium ions in our bare nanoparticle studies as well.

Since the formation of a "water finger" or network of water molecules is crucial for ion permeation, we chose to examine the difference in the formation of the water pore during permeation by a bare NP and a LCNP. In Figures 9 and 10, we present snapshots of the water column formed between the aqueous compartment A and compartment B of our system at the stage when the number of water molecules in the hydrophobic membrane interior has reached a maximum for 2 and 3 nm particles, respectively. We have already seen in Figures 2 and 3 that the number of water molecules leaked into the membrane interior reaches a maximum when the ligands of the nanoparticle have completely exited the second leaflet of the membrane bilayer, unlike the case of the bare NP, in which this occurs when the nanoparticle has just moved past the position of the phosphate groups of the lower leaflet of the membrane.

In Figure 9a-−c, we observe the water column formation for 3.0 nm diameter nanoparticle permeation in the bare and ligand-coated cases. During permeation of a bare nanoparticle, a very distinct water column is formed on which ions can travel to the bottom system compartment across the bilayer membrane. We do discern the formation of a noticeable water column in Figure 10a, which explains why we observed the number of ions permeating increase with increasing size of the bare NP. For the 2 nm particle (Figure 9a), the finger is clearly not as well formed, and thus, we see few ion penetration events for varying system conditions. For the 3.0 nm diameter SL-LCNP, however, we see a less noticeable water column, and at higher ligand lengths, the water finger is not observed at all. If we compare Figure 10c with Figure 3c,f, there appears to be an apparent inconsistency because the water penetration for LL-LCNP was relatively high. We would like to reiterate that water penetration occurs from both the top and bottom leaflets. In the case of the LL-LCNP, most of the water penetration is from the lower leaflet, which explains the relatively high water penetration, despite the absence of a water finger. For the LL-LCNP, we observed few to no ion transport events, which is consistent with our observation of no distinct water column formation, as seen in Figure 10c. This is due to the disturbance of the membrane by the mobile long ligands on the nanoparticle that push lipid and water molecules away from the nanoparticle core; since a long-lived water column is unable to form, fewer ions are able to permeate the lipid bilayer. Because our system models the permeation of only one nanoparticle, the lifetime of the water pore formed is quite short (50−100 ns), and the lipid bilayer begins to recover before thermodynamic equilibrium can be reached. If multiple particle insertions were to take place over an extended period of time, then ultimately, the concentration of the top and bottom compartment would be in thermodynamic equilibrium with equal concentrations.

4.0. CONCLUSIONS

In this study, we have carefully examined the effects of nanoparticle permeation on a model DPPC lipid bilayer membrane. These studies simulate events that may occur at the cell membrane during practical applications of drug delivery using nanoparticle carriers. Our studies have shown that when ligand-coated nanoparticles permeate lipid membranes, water and ion leakage, lipid flip-flop, and lipid loss from the membrane can occur. These permeation effects can contribute to cell cytotoxicity and can have negative implications for nanoparticle drug delivery systems. The mechanism for lipid flip-flop accompanying particle penetration is essentially unchanged from our previous work, although far fewer such events go to completion because of lipid entanglement with the ligands attached to the nanoparticle. At the same time, the latter leads to loss of lipids from the membrane. We demonstrated the mechanism for lipid loss from the bilayer: as the nanoparticle approaches the top layer of the membrane, even before it begins to create a water pore, two of its hydrophobic ligands can interact with a lipid molecule and drag it along, so the lipid is unable to complete a flip-flop to rejoin the membrane; instead, it remains entangled and leaves with the NP as it moves through to the other side. This happens more frequently with larger particles and longer ligands. The loss of lipid molecules from a cellular membrane can affect membrane integrity and, hence, the physiological environment of the cell, which can ultimately result in cellular death. It is worthwhile to note that ligand-coated nanoparticles typically used for drug delivery are in some ways less disruptive (fewer ion-penetration and flip-flop events) to lipid membranes than bare nanoparticles, such as those that may accompany grinding or other dry surface abrading operations. The only exception to this general observation is lipid loss during the permeation process. Our results, which compare the permeation effects of functionalized nanoparticles under various conditions, can aid in developing nanoparticle carriers that will minimize the cytotoxic effects.

AUTHOR INFORMATION

Corresponding Author

*Phone: (312)- 567-3867. E-mail: murad@iit.edu.

Notes

The authors declare no competing financial interest.

ACKNOWLEDGMENTS

This research has been funded by a grant from the National Science Foundation (Grant No. CBET-0730026/1263107). We thank Drs. Bo Song and Huajun Yuan for many helpful discussions during the course of this research.

REFERENCES

(1) Chithrani, B. D.; Chan, W. C. Elucidating the mechanism of cellular uptake and removal of protein-coated gold nanoparticles of different sizes and shapes. *Nano Lett.* **2007**, *7* (6), 1542−1550.

(2) Chithrani, B. D.; Ghazani, A. A.; Chan, W. C. W. Determining the size and shape dependence of gold nanoparticle uptake into mammalian cells. *Nano Lett.* **2006**, *6* (4), 662−668.

(3) Jiang, W.; Kim, B. Y.; Rutka, J. T.; Chan, W. C. Nanoparticle-mediated cellular response is size-dependent. *Nat. Nanotechnol.* **2008**, *3* (3), 145−50.

(4) Leroueil, P. R.; Berry, S. A.; Duthie, K.; Han, G.; Rotello, V. M.; McNerny, D. Q.; Baker, J. R.; Orr, B. G.; Banaszak Holl, M. M. Wide varieties of cationic nanoparticles induce defects in supported lipid bilayers. *Nano Lett.* **2008**, *8* (2), 420−424.

(5) Bhattacharya, S.; Srivastava, A. Synthesis and characterization of novel cationic lipid and cholesterol-coated gold nanoparticles and their

DOI: 10.1021/la503934c
Langmuir 2015, 31, 1074−1085

interactions with dipalmitoylphosphatidylcholine membranes. *Langmuir* **2003**, *19* (10), 4439−4447.
(6) Hostetler, M. J.; Templeton, A. C.; Murray, R. W. Dynamics of place-exchange reactions on monolayer-protected gold cluster molecules. *Langmuir* **1999**, *15* (11), 3782−3789.
(7) Hainfeld, J. F.; Slatkin, D. N.; Smilowitz, H. M. The use of gold nanoparticles to enhance radiotherapy in mice. *Phys. Med. Biol.* **2004**, *49* (18), N309−N315.
(8) Park, S.-H.; Oh, S.-G.; Mun, J.-Y.; Han, S.-S. Loading of gold nanoparticles inside the DPPC bilayers of liposome and their effects on membrane fluidities. *Colloids Surf., B* **2006**, *48* (2), 112−118.
(9) Lin, J.; Zhang, H.; Chen, Z.; Zheng, Y. Penetration of lipid membranes by gold nanoparticles: Insights into cellular uptake, cytotoxicity, and their relationship. *ACS Nano* **2010**, *4* (9), 5421−5429.
(10) Verma, A.; Uzun, O.; Hu, Y.; Hu, Y.; Han, H.-S.; Watson, N.; Chen, S.; Irvine, D. J.; Stellacci, F. Surface−structure-regulated cell-membrane penetration by monolayer-protected nanoparticles. *Nat. Mater.* **2008**, *7* (7), 588−595.
(11) Ghosh, P.; Han, G.; De, M.; Kim, C. K.; Rotello, V. M. Gold nanoparticles in delivery applications. *Adv. Drug Delivery Rev.* **2008**, *60* (11), 1307−1315.
(12) Song, B.; Yuan, H.; Pham, S. V.; Jameson, C. J.; Murad, S. Nanoparticle permeation induces water penetration, ion transport, and lipid flip-flop. *Langmuir* **2012**, *28* (49), 16989−17000.
(13) Guo, S.; Wang, E. Synthesis and electrochemical applications of gold nanoparticles. *Anal. Chim. Acta* **2007**, *598* (2), 181−192.
(14) Li, Y.; Chen, X.; Gu, N. Computational investigation of interaction between nanoparticles and membranes: hydrophobic/hydrophilic effect. *J. Phys. Chem. B* **2008**, *112* (51), 16647−16653.
(15) Lee, O. S.; Schatz, G. C. Computational simulations of the interaction of lipid membranes with DNA-functionalized gold nanoparticles. *Methods Mol. Biol.* **2011**, *726*, 283−296.
(16) Lin, J.-Q.; Zheng, Y.-G.; Zhang, H.-W.; Chen, Z. A simulation study on nanoscale holes generated by gold nanoparticles on negative lipid bilayers. *Langmuir* **2011**, *27* (13), 8323−8332.
(17) Ding, H.-m.; Tian, W.-d.; Ma, Y.-q. Designing nanoparticle translocation through membranes by computer simulations. *ACS Nano* **2012**, *6* (2), 1230−1238.
(18) Fiedler, S. L.; Violi, A. Simulation of nanoparticle permeation through a lipid membrane. *Biophys. J.* **2010**, *99* (1), 144−152.
(19) Monticelli, L.; Kandasamy, S. K.; Periole, X.; Larson, R. G.; Tieleman, D. P.; Marrink, S.-J. The MARTINI coarse-grained force field: Extension to proteins. *J. Chem. Theory Comput.* **2008**, *4* (5), 819−834.
(20) Marrink, S. J.; Risselada, H. J.; Yefimov, S.; Tieleman, D. P.; de Vries, A. H. The MARTINI force field: Coarse grained model for biomolecular simulations. *J. Phys. Chem. B* **2007**, *111* (27), 7812−7824.
(21) Yuan, H.; Jameson, C. J.; Murad, S. Diffusion of gases across lipid membranes with OmpA channel: A molecular dynamics study. *Mol. Phys.* **2010**, *108* (12), 1569−1581.
(22) Song, B.; Yuan, H.; Jameson, C. J.; Murad, S. Role of surface ligands in nanoparticle permeation through a model membrane: A coarse-grained molecular dynamics simulations study. *Mol. Phys.* **2012**, *110* (18), 2181−2195.
(23) Goodman, C. M.; McCusker, C. D.; Yilmaz, T.; Rotello, V. M. Toxicity of gold nanoparticles functionalized with cationic and anionic side chains. *Bioconjugate Chem.* **2004**, *15* (4), 897−900.
(24) Pan, Y.; Neuss, S.; Leifert, A.; Fischler, M.; Wen, F.; Simon, U.; Schmid, G.; Brandau, W.; Jahnen-Dechent, W. Size-dependent cytotoxicity of gold nanoparticles. *Small* **2007**, *3* (11), 1941−1949.
(25) Hostetler, M. J.; Wingate, J. E.; Zhong, C.-J.; Harris, J. E.; Vachet, R. W.; Clark, M. R.; Londono, J. D.; Green, S. J.; Stokes, J. J.; Wignall, G. D.; Glish, G. L.; Porter, M. D.; Evans, N. D.; Murray, R. W. Alkanethiolate gold cluster molecules with core diameters from 1.5 to 5.2 nm: Core and monolayer properties as a function of core size. *Langmuir* **1998**, *14* (1), 17−30.
(26) Tanaka, M.; Sackmann, E. Polymer-supported membranes as models of the cell surface. *Nature* **2005**, *437* (7059), 656−663.
(27) Song, B.; Yuan, H.; Jameson, C. J.; Murad, S. Permeation of nanocrystals across lipid membranes. *Mol. Phys.* **2011**, *109* (11), 1511−1526.
(28) Forbes, Z. G.; Yellen, B. B.; Halverson, D. S.; Fridman, G.; Barbee, K. A.; Friedman, G. Validation of high gradient magnetic field based drug delivery to magnetizable implants under flow. *IEEE Trans. Biomed. Eng.* **2008**, *55* (2), 643−649.
(29) Wang, S.; Zhou, Y.; Tan, J.; Xu, J.; Yang, J.; Liu, Y. Computational modeling of magnetic nanoparticle targeting to stent surface under high gradient field. *Comput. Mech.* **2014**, *53* (3), 403−412.
(30) Grief, A. D.; Richardson, G. Mathematical modelling of magnetically targeted drug delivery. *J. Magn. Magn. Mater.* **2005**, *293* (1), 455−463.
(31) Petros, R. A.; DeSimone, J. M. Strategies in the design of nanoparticles for therapeutic applications. *Nat. Rev. Drug Discovery* **2010**, *9* (8), 615−627.
(32) Wang, J.; Byrne, J. D.; Napier, M. E.; DeSimone, J. M. More effective nanomedicines through particle design. *Small* **2011**, *7* (14), 1919−1931.
(33) Arai, N.; Yasuoka, K.; Zeng, X. C. A vesicle cell under collision with a Janus or homogeneous nanoparticle: Translocation dynamics and late-stage morphology. *Nanoscale* **2013**, *5* (19), 9089−9100.
(34) Bennett, W. F.; Sapay, N.; Tieleman, D. P. Atomistic simulations of pore formation and closure in lipid bilayers. *Biophys. J.* **2014**, *106* (1), 210−219.
(35) Tieleman, D. P.; Leontiadou, H.; Mark, A. E.; Marrink, S.-J. Simulation of pore formation in lipid bilayers by mechanical stress and electric fields. *J. Am. Chem. Soc.* **2003**, *125* (21), 6382−6383.
(36) Plimpton, S. Fast parallel algorithms for short-range molecular dynamics. *J. Comput. Phys.* **1995**, *117* (1), 1−19.
(37) Roiter, Y.; Ornatska, M.; Rammohan, A. R.; Balakrishnan, J.; Heine, D. R.; Minko, S. Interaction of nanoparticles with lipid membrane. *Nano Lett.* **2008**, *8* (3), 941−944.
(38) Chen, J.; Hessler, J. A.; Putchakayala, K.; Panama, B. K.; Khan, D. P.; Hong, S.; Mullen, D. G.; DiMaggio, S. C.; Som, A.; Tew, G. N.; Lopatin, A. N.; Baker, J. R.; Holl, M. M. B.; Orr, B. G. Cationic nanoparticles induce nanoscale disruption in living cell plasma membranes. *J. Phys. Chem. B* **2009**, *113* (32), 11179−11185.
(39) Lee, H.; Larson, R. G. Molecular dynamics simulations of PAMAM dendrimer-induced pore formation in DPPC bilayers with a coarse-grained model. *J. Phys. Chem. B* **2006**, *110* (37), 18204−18211.
(40) Lee, H.; Larson, R. G. Lipid bilayer curvature and pore formation induced by charged linear polymers and dendrimers: The effect of molecular shape. *J. Phys. Chem. B* **2008**, *112* (39), 12279−12285.
(41) Lee, H.; Larson, R. G. Coarse-grained molecular dynamics studies of the concentration and size dependence of fifth- and seventh-generation PAMAM dendrimers on pore formation in DMPC bilayer. *J. Phys. Chem. B* **2008**, *112* (26), 7778−7784.
(42) Gurtovenko, A. A.; Vattulainen, I. Pore formation coupled to ion transport through lipid membranes as induced by transmembrane ionic charge imbalance: Atomistic molecular dynamics study. *J. Am. Chem. Soc.* **2005**, *127* (50), 17570−17571.
(43) Tieleman, D. P.; Marrink, S.-J. Lipids Out of Equilibrium: Energetics of desorption and pore mediated flip-flop. *J. Am. Chem. Soc.* **2006**, *128* (38), 12462−12467.
(44) Gurtovenko, A. A.; Vattulainen, I. Molecular mechanism for lipid flip-flops. *J. Phys. Chem. B* **2007**, *111* (48), 13554−13559.
(45) Gurtovenko, A. A.; Vattulainen, I. Ion leakage through transient water pores in protein-free lipid membranes driven by transmembrane ionic charge imbalance. *Biophys. J.* **2007**, *92* (6), 1878−1890.
(46) Gurtovenko, A. A.; Onike, O. I.; Anwar, J. Chemically induced phospholipid translocation across biological membranes. *Langmuir* **2008**, *24* (17), 9656−9660.
(47) Higgins, C. F. Flip-flop: the transmembrane translocation of lipids. *Cell* **1994**, *79* (3), 393−395.

DOI: 10.1021/la503934c
Langmuir 2015, 31, 1074−1085

(48) Devaux, P. F. Lipid transmembrane asymmetry and flip-flop in biological membranes and in lipid bilayers. *Curr. Opin. Struct. Biol.* **1993**, *3* (4), 489−494.
(49) Contreras, F.; Sánchez-Magraner, L.; Alonso, A.; Goñi, F. M. Transbilayer (flip-flop) lipid motion and lipid scrambling in membranes. *FEBS Lett.* **2010**, *584* (9), 1779−1786.
(50) Wallace, E. J.; Sansom, M. S. Blocking of carbon nanotube based nanoinjectors by lipids: A simulation study. *Nano Lett.* **2008**, *8* (9), 2751−2756.
(51) Khavrutskii, I. V.; Gorfe, A. A.; Lu, B.; McCammon, J. A. Free energy for the permeation of Na^+ and Cl^- Ions and their ion-pair through a zwitterionic dimyristoyl phosphatidylcholine lipid bilayer by umbrella integration with harmonic fourier beads. *J. Am. Chem. Soc.* **2009**, *131* (5), 1706−1716.
(52) Benjamin, L. Mechanism and dynamics of ion transfer across a liquid-liquid interface. *Science (New York, NY)* **1993**, *261* (5128), 1558−1560.
(53) Schweighofer, K. J.; Benjamin, I. Electric field effects on the structure and dynamics at a liquid|liquid interface. *J. Electroanal. Chem.* **1995**, *391* (1), 1−10.
(54) Luo, G.; Malkova, S.; Yoon, J.; Schultz, D. G.; Lin, B.; Meron, M.; Benjamin, I.; Vanýsek, P.; Schlossman, M. L. Ion distributions near a liquid−liquid interface. *Science* **2006**, *311* (5758), 216−218.
(55) Wilson, M. A.; Pohorille, A. Mechanism of unassisted ion transport across membrane bilayers. *J. Am. Chem. Soc.* **1996**, *118* (28), 6580−6587.
(56) Yamashita, T.; Voth, G. A. Properties of hydrated excess protons near phospholipid bilayers. *J. Phys. Chem. B* **2009**, *114* (1), 592−603.
(57) Mancinelli, R.; Botti, A.; Bruni, F.; Ricci, M. A.; Soper, A. K. Hydration of sodium, potassium, and chloride ions in solution and the concept of structure maker/breaker. *J. Phys. Chem. B* **2007**, *111* (48), 13570−13577.

DOI: 10.1021/la503934c
Langmuir 2015, 31, 1074−1085